The effect of long-range order on intermolecular interactions in organic semiconductors: Zinc octaethyl porphyrin molecular thin film model systems

Effect of long-range order on Intermolecular Interactions in Organic Semiconductors: Zinc octa ethyl porphyrin molecular thin films model systems

A. Kumar,*[a,b] D. Naumenko,*[c] G. Rossi,[d] E. Magnano, [a] S. Nappini, [a] F. Bondino, [a] E. Segoloni, [a] L. Amidani, [d,^], F. d'Acapito, [e] F. Boscherini, [d] L. Barba, [f] E. Pace,[g] M. Benfatto, [g] S. Casassa, [h] and M. Pedio [a]

[a] Istituto Officina dei Materiali, Consiglio Nazionale delle Ricerche, TASC Laboratory, Trieste, Italy
[b] Dipartimento di Fisica, Università di Trieste, Trieste I-34127, Italy
[c] Elettra Sincrotrone Trieste, Area Science Park Basovizza, Trieste 34149, Italy
[d] Department of Physics and Astronomy, University of Bologna, Italy
[e] Istituto Officina dei Materiali, Consiglio Nazionale delle Ricerche, c/o ESRF, Grenoble, France
[f] Istituto CNR- IC, Area Science Park Basovizza, Trieste, 34149, ITALY
[g] LNF-INFN Frascati 00044 Italy
[h] Dipartimento di Chimica, Università di Torino and NIS, Nanostructured Interfaces and Surfaces, Centre of Excellence, Via Giuria 5, 10125 Torino, Italy

[^] Present address: ROBL beamline at ESRF, Grenoble, France.
*These authors contributed equally to this work.

Abstract

It is crucial to understand various factors influencing the charge transport and light-harvesting ability of porphyrin thin films for the improvement of porphyrin based devices. In this work, we have employed vacuum deposited Zinc OctaEthyl Porphyrin (ZnOEP) thin films with a different degree of long-range order as model systems. An asymmetrical stretching of skeletal carbon atoms of the porphyirn conformer has been observed attributed by the ordered molecular stacking and intermolecular interactions. Detailed MXAN fitting analysis of X-ray absorption near edge structure (XANES) establishes a symmetry reduction in the molecular conformer involving skeletal carbon atoms of the porphyirn ring for the ordered films highlighting the consequences of increased π stacking of ZnOEP molecules adopting triclinic structure. The observed unsymmetrical stretching of π conjugation network of porphyrin structure can have significant implications on the charge transport and light harvesting ability of porphyrin thin films, notably impacting the performances of porphyrin based devices.

Keywords Organic Semiconductors, Porphyrins thin Film, x-ray absorption spectroscopy, Intermolecular interaction

Introduction

Among tetrapyrrole complexes, porphyrin molecules have found applications in optoelectronic devices such as organic field-effect transistors (OFETs), organic photovoltaic devices, and organic light-emitting diodes (OLEDs)[1]. Porphyrin related molecules exhibit rich optical absorption features in the visible region, therefore have been utilized extensively as photosensitizers in dye sensitized solar cells[2]. Due to such impactful applications, considerable attention has been given to various factors influencing charge carrier mobility and light harvesting ability of porphyrin molecular thin films. Theoretical calculations show that optical properties of porphyrin molecules are strongly dependent on the π conjugation network.[3] It has been observed that the elongation of the π conjugation and loss of symmetry in porphyrins cause broadening and a red shift of the absorption bands together with an increasing intensity of the Q bands (500-600nm) relative to that of the Soret band (near 400 nm) [2]

Light harvesting ability and transport of porphyrin thin films are influenced by the molecular packing and long range order. It is evident from fig.1(c) that relative intensity of Q bands is higher than Soret band for semiordered crystalline ZnOEP films on the transparent substrate ITO as compared to disordered film. Further, the optical absorption spectra obtained

in solution[4] and gas phase[5] are notably different than semiordered crystalline ZnOEP films on ITO highlighting the impact of unique molecular packing and long range order as shown in Fig.1(c).

The photoenergy conversion efficiency has been found to be related to long-range order in ZnOEP films[6,7]. In case of C_{60}-ZnOEP heterojunctions the hole mobility in the ZnOEP film becomes higher by crystallization[8], increasing the number of inter-molecular charge-transfer (IMCT) excitons and enlarging the mobility of carriers. It results in significant improvement of photoabsorption band efficiency under illumination.

Molecular orientation, crystallinity and intermolecular interactions of the organic semiconductors TF significantly impact their transport properties. The diffusion length of excitons and/or charge carriers mobilities are found to be larger in crystalline films than in their amorphous forms[9,10], while quantum-chemical calculations confirm that molecular packing, density of chemical and/or structural defects significantly influence charge transport in organic semiconductors[11]. Further, in Metal Octaethyl Porphyrin (MOEP) triclinic crystals with various central metal atoms, the field-effect mobility of porphyrin-based field-effect transistors have been found to increase with decreasing intermolecular distance.[12] Field effect mobility has been found to be dependent on molecular orientation: vertically aligned Platinum OctaEthyl Porphyrin (PtOEP) molecules (edge-on) show 100 times higher field effect mobility as compared to horizontally aligned (flat–on) PtOEP molecules. [13] ZnOEP aggregates as nanorods, films, nanowire blends in polymer films[14,15,16,17] have recently received strong interest and the π-π intermolecular interactions in the triclinic structure have been considered the driving force of the molecular stacking in the solid ZnOEP aggregates.

Moreover, it has been observed that proximity of ethyl groups in the triclinic structure of ZnOEP influences their vibrational properties. Notably, Infrared vibrational spectroscopy investigation together with X-ray diffraction study for the ZnOEP thin films on quartz substrate reveal that asymmetric vibration of CH_3 gets hindered due to proximity with the CH_2 of the neighboring ZnOEP molecule and results in the suppression of IR peak due to asymmetric vibration of CH_3 (1446cm^{-1}). This peak gets restored for amorphous ZnOEP/C_{60} films highlighting the impact of intermolecular interaction on properties of ZnOEP thin films.[18]

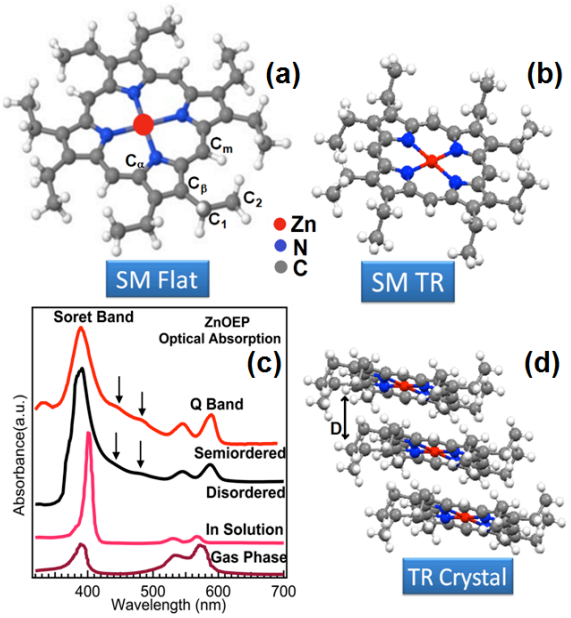

Figure 1 The ZnOEP conformers: SM Flat isolated flat molecule, SM TR ZnOEP with out of plane ethyl groups orientation within the triclinic structure, TR Crystal the same conformer in the triclinic structure. D indicates the adiacent plane distance(~ 3.4 Å). The optical absorption spectra of disordered and semiordered ZnOEP TF on ITO are compared with literature spectra of gas phase and solution ZnOEP dissolved in dichloromethane . Peaks labeled with arrows are related to the inter-molecular charge-transfer excitons in the films [7].

ZnOEP molecule can adopt two conformers that differ in mutual orientations of ethyl groups. These are alternatively oriented for the isolated free molecule, labeled SM flat in Fig. 1 (gas phase and solutions). In the solid triclinic structure, labeled SM TR the ethyl-groups are in a *trans* configuration with respect to the basal plane with four ethyl groups pointing upward, while the other four pointing downward, probably to reduce steric (and repulsion) effects in solids. Generally, porphyrins present a pronounced tendency to polymorphism in crystal packing. At variance the ZnOEP, considered a good model system[19], has no structural polymorphism in the single crystal[20,21] presenting the triclinic structure, labelled TR in Fig. 1.

In order to highlight the impact of unique molecular packing and long range order to π conjugation network, we adopt multi-technique characterization to gain complementary information

on vibrational properties and degree of order/dimension of the crystallites in the film using Raman spectroscopy, grazing incidence X-ray diffraction (GIXRD) and atomic force microscopy (AFM). X-ray absorption fine structure (XAFS) plays an important role in elucidating the local atomic structure by isong the protocol established for the molecular characterization in TF in ref. [22]. Our results indicate that the degree of order in the ZnOEP films is determined by the substrate, its treatment and by the growth procedures. We found that the increasing of long range order, leading to greater overlap of π orbitals, is also related to the symmetry reduction of ZnOEP conformers involving the outer C_β and C_α and ethyl carbon atoms.

Methods

The bulk sample was commercial high purity ZnOEP polycrystalline powder (Sigma Aldrich). ZnOEP TF, thickness ~40 nm, were deposited *ex – situ* by sublimation in UHV, deposition rate of ~ 2 Å/min (base pressure 2 10^{-10} mbar, pressure during deposition 5 10^{-9} mbar) from resistively heated quartz crucibles containing ZnOEP powders. The thickness was measured by oscillating quartz microbalances. The ZnOEP molecules were deposited at room temperature (RT) on native SiOx/Si and Indium tin oxide (ITO) substrates, with roughness of 0.2 nm and 1.7 nm respectively. The ITO substrates were rinsed in acetone before introducing them in the UHV chamber. The Silicon substrates with 40 Å of native oxide (SILTRONIX), were used as raw or in some case annealed at 300°C in UHV. In order to increase the ordering the annealing of the TF was performed after deposition at temperature far below the sublimation point at a mild thermal annealing of the ZnOEP TF at 80 °C for 10 hours in UHV. All the measurements on ex-situ sample have been performed on fresh prepared samples. The ZnOEP TFs deposited on ITO at RT are labeled as “disordered” and “semiordered” on SiOx/Si. While annealed TFs on ITO are labeled as “semiordered” and annealed TF on SiOx/Si are labeled as “ordered”.

XAFS measurements at Zn K edge were performed at the “GILDA/LISA” BM-08 beamline[23] of the European Synchrotron Radiation Facility (ESRF Grenoble France). The films were measured in the fluorescence mode using a dynamically sagitally focusing Si (311) monochromator, a hyper pure Ge detector and associated digital electronics with a 1 µs peaking time[24]. Higher order harmonics were eliminated with a pair of Pd coated grazing incidence mirrors. The energy spacing for the EXAFS spectra was equivalent to less than 0.05 $Å^{-1}$.

The NEXAFS spectra of the nitrogen K-edge and X-ray photoelectron spectroscopy (PES) measurements were carried out at the CNR beamline BACH at Elettra in a base pressure < 10^{-9} mbar[25]. NEXAFS spectra were measured both in fluorescence yield (FY) using a multi channel plate (MCP) detector (F4655 Hamamatsu) and in total electron yield (TEY), ensuring either bulk or surface sensitivities, respectively. The main core levels and the photon energy calibration were evaluated by PES measurements using a VG Scienta R3000 hemispherical electron analyzer.[26] A photon energy of 600 eV, corresponding to an inelastic mean free path in the range of 1 nm, was employed to compare the composition and contamination of *in-situ* and *ex-situ* samples .

The Zn K edge XANES spectra have been simulated by means of the MXAN code[27], by using the full multiple scattering (MS) approach within the muffin tin (MT) approximation. The real part of the exchange and correlation potential has been calculated on the basis of the Hedin-Lundqvist approximation, inelastic losses are taken into account. The zero-energy corresponds to the interstitial potential of the muffin-tin spheres. Muffin-tin radii and the interstitial potential have been optimized during the fitting procedure[28]. The best fit condition is obtained by minimization of the R_{sq} function of the ion taken as likelihood parameter as defined in ref. 27.

GIXRD measurements were performed at the X-ray Diffraction beamline 5.2 at the Synchrotron Radiation Facility Elettra (Trieste, Italy)[29] following the standard procedures[30]. The detailed information regarding GIXRD, AFM and Raman instrumentation along with approach adopted for simulating Raman spectra are mentioned in supporting information.

Results and discussion

Fig. 2 shows the bidimensional diffraction patterns for the ZnOEP films: (a) TF deposited at RT and then

annealed on SiOx/Si,(b) TF deposited at RT on SiOx/Si, (c) TF deposited on ITO and successively annealed and (d) TF deposited at RT on ITO. GIXRD measurements certainly demonstrate the differences in the long range order for the as deposited ZnOEP TF. Multiple diffraction spots are clearly detectable for the annealed ZnOEP TF on SiOx/Si demonstrating highly crystalline and ordered structure. The diffraction spots are comparatively spread for the ZnOEP TF deposited at RT on SiOx/Si demonstrating a lower molecular order of ZnOEP molecules, therefore termed as semiordered. Almost similar behaviour has been observed for TF deposited on ITO and successively annealed. It demonstrates level of randomness in the molecular stacking for these TFs. Almost no detectable diffraction spots are visible for ZnOEP TF deposited at RT on ITO. This confirms that crystalline order is poor and ZnOEP molecules are randomly oriented on ITO. The rings in the bottom panels c) and d) are related to the ITO substrate disordered structures while Si bulk reflections are visible as spots in a hexagonal arrangement in the upper panels.

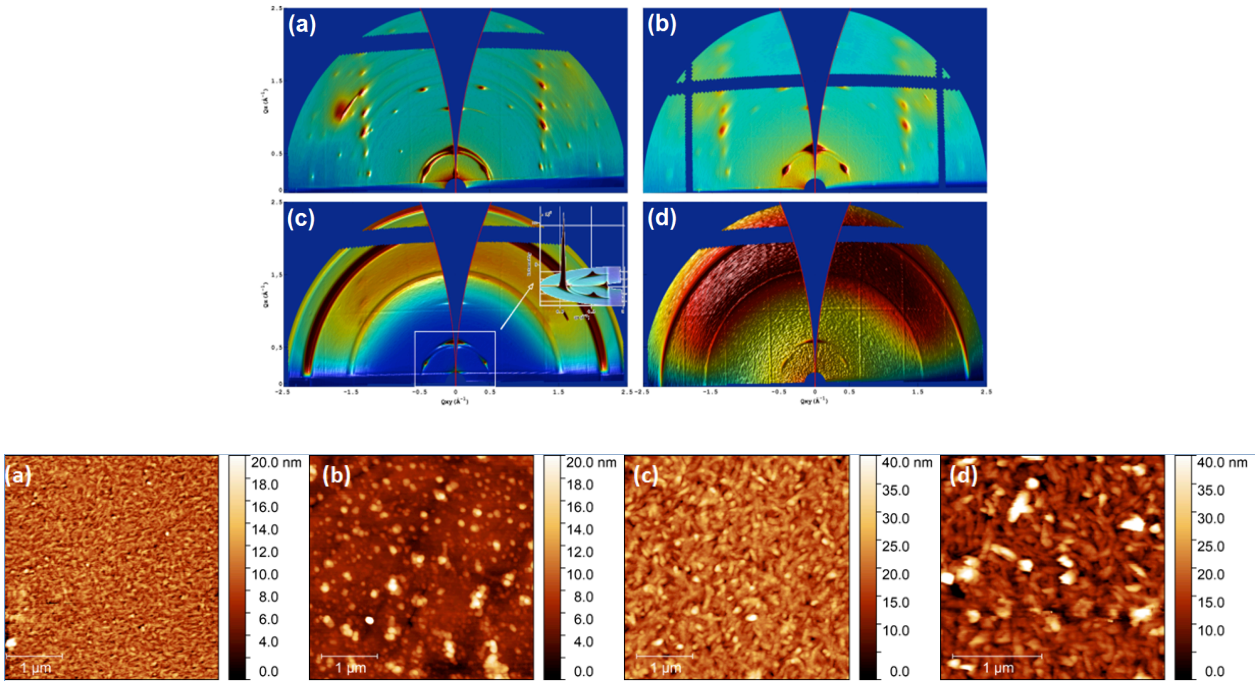

Figure 2 Top Panel **:** Bidimensional diffraction patterns on the ZnOEP films a) ordered sample on SiOx/Si, b) semiordered on SiOx/Si c) semiordered annealed sample on ITO and d) disordered sample on ITO. The indexing has been assigned through the powder simulated XRD pattern (Mercury code) from reported data[20].Bottom Panel: AFM images of ZnOEP films deposited on (a) ordered (b) semiordered/Si (C) semiordered/ITO and (d) disordered film.

Sample	GIXRD Average crystallite volume weighted Size nm	Paracrystallinity	AFM Average grain size nm	AFM RMS (Roughness) nm
Ordered	24.0 nm	2.75	20.2	2.25
Semiordered/Si	25.8 nm	4.73	39.3	2.52
Semiordered/ITO	28.5 nm	5.88	39.4	4.42
Disordered/ITO	No data	No data	45.5	7.39

Table 1: Average grain size as result from AFM compared with the crystallites size as obtained from GIXRD peak profile analysis. AFM resulting roughness is also reported. Average crystallite size and microstrains derived from the first four peaks of crystallographic family 0 0 L according to Hosemann paracrystal theory. Crystallites' size is related to the coherence length in the specified crystallographic direction.

Cell parameters were checked against reference data[20] by means of the Mercury code. Peak positions were extracted by means of Fit2d in association with WinPlotr. Our GIXRD analysis shows that the reported triclinic structure[6-8,15,16] of the ZnOEP single crystal[20] is compatible with the reflection sets measured in

our samples, with the reported peak positions that can be indexed as the triclinic lattice with a =4.692 Å, b =13.185 Å, c =13.287 Å, α=113.94, β=91.177 and γ=92.16. In all the cases the first order (higher intensity) reflections are detectable, even in the disordered sample and exhibits good resemblance with the results obtained by laboratory sources. The dominant orientation of crystallites for ordered, semiordered and disordered ZnOEP thin films is along (01-1).

Peak profile analysis has been performed after indexing the patterns, by the Hosemann model [31]. The results are summarized in Table 1 for the 00L reflections.Average crystallite size is lower for semiordered film on SiOx/Si substrate as compared to ITO which can be attributed to the different growth mechanism induced by dissimilar surface roughness and molecule-substrate interactions. Paracrystallinity is least for the ordered film on SiOx/Si, while it is higher for the disordered film grown on ITO as compared to semiordered film on SiOx/Si indicating towards higher disorder with in grain for the ZnOEP deposition on ITO.

AFM images were analyzed using average crystallite size and root mean square (RMS) parameters as listed in Table 1 and reveal smaller grain size and lower surface roughness for the ordered film testifying about higher order of ZnOEP crystallites on SiO_x/Si surface as shown in Fig.2. In order to have a quantitative characterization of the films the Power Spectral Density function (Figure SI-1) provides a representation of the amplitude of a surface's roughness as a function of the spatial frequency of the roughness. The evaluated crystallite size of ordered ZnOEP TF is 20.2 nm while semiordered (both for ITO and SiOx substrates) it is about 39.4 nm. Although, the AFM grain sizes follow the similar trend as crystallite sizes measured by X-ray diffraction, the AFM grain sizes show higher value as compared to crystallite sizes. This is because AFM micrograph, which is obtained by scanning the topography of the surface, provides information about agglomerated crystallites i.e. domain of crystallites[32]. On the other hand, reported crystallite sizes by GIXRD are related to the coherent scattering domain having perfect molecular order of unit cells in the specified crystallographic direction. Thus, combined GIXRD and AFM analyses show that the ZnOEP TF are formed of crystallites whose size results decreased in case of ordered films, while the paracrystallinity improves. Similar trend of higher Paracrystallinity and grain size have been observed for phthalocyanine TFs[33] .

Raman spectroscopy characterization (Fig. 3) provides the vibrational properties of the ZnOEP TF. Ab-initio calculations has been performed to simulate Raman spectra after the structural optimization of ZnOEP molecule at B3LYP-D* level. ZnOEP structural optimization confirms the *trans* configuration (Fig. 1). The detailed assignment of the peaks along with calculated Raman bands can be seen in table (SI-2). [34,35] As shown in Fig.3 a) no Raman shift for the vibrational modes involving central metal atom bound to 4 N atoms in the macrocycle suggests that in spite of dissimilar paracrystallinity and hence molecular stacking, no significant structural changes occur in the macrocycle and intermolecular interactions in the closely packed ordered films (triclinic structure) do not lead to macrocycle deformation. However, for skeletal carbon atoms (C_β, C_m, C_α) vibrational modes, we observe small but notable Raman shift indicating a probable structural deformations related to (C_β, C_m, C_α). Such Raman shifts related to vibrational bands at 1561 cm^{-1}($C_\beta C_\beta$), 1621 cm^{-1}($C_\alpha C_m$) and 1376 cm^{-1}($C_\alpha N$) due to π-π interactions have been observed for CuOEP[36] and zinc(II) and palladium(II) octakis(βdecoxyethyl) porphyrins[37].

Notably, there is a significant decrease in the intensity of vibrational modes related to C-N-Zn (357cm^{-1}) and Zn-N_4 (254cm^{-1}) and 1561 cm^{-1} ($C_\beta C_\beta$), 1621 cm^{-1} ($C_\alpha C_m$) and 1376 cm^{-1} ($C_\alpha N$) for disordered film as compared to ordered film.

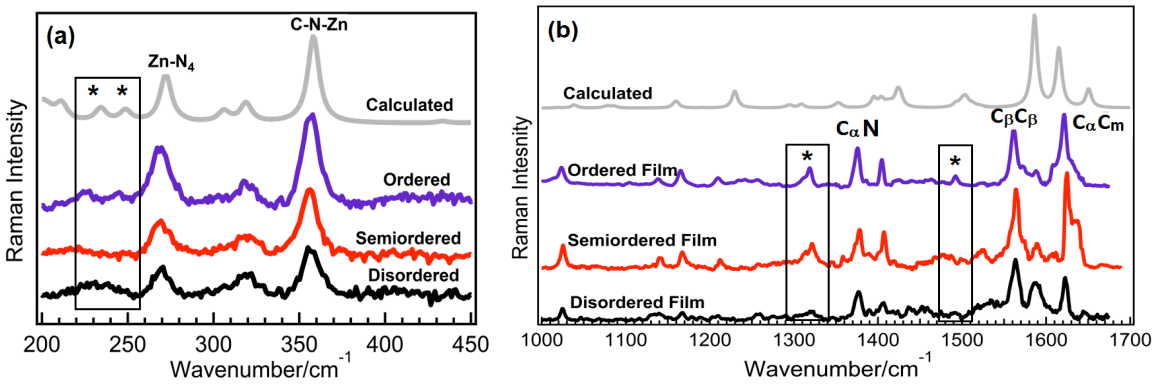

Figure 3. The Raman spectra of ZnOEP films acquired at 532 nm excitation wavelength within (a) 200-450 cm^{-1} and within (b) 1000 -1700 cm^{-1} compared with the theoretical calculation of frozen ZnOEP molecule. Peaks labeled as * are related to peripheral ethyl groups vibrational modes.

Due to dissimilar molecular stacking and higher disorder of ZnOEP molecules, the intensity of Raman bands is least for disordered TFs deposited at RT on ITO. Such a sensitive dependence of macrocycle vibrational band intensities for the disordered film has been reported for Titanyl Phthalocyanine TF grown on amorphous quartz plates at different temperature[38]. Disordered molecular stacking of iron and cobalt phthalocyanine (FePc and CoPc) TFs deposited on ITO has been revealed by the dependence of macrocycle vibrational band intensity on molecular order.[33] In the low frequency range simulated Raman spectrum shows good agreement with observed ordered film spectrum as shown in the Fig.3a. Two distinguishable peaks at 225 cm^{-1} (calculated 234cm^{-1}) and 245 cm^{-1} (calculated 249cm^{-1}) are related ethyl groups vibrational modes.[35] In addition, modes at 1320cm^{-1} and 1492cm^{-1} are also related to peripheral ethyl group vibrations. Calculations reveal that the anti-phase bending motions of the CH_3 and CH_2 moieties give rise to the set of peaks concentrated around 1500 cm^{-1} that has been experimentally observed as a single peak at 1492 cm^{-1} only in case of ordered film deposited in SiOx/Si. As shown in Fig. 3 (a) and (b) vibrational modes corresponding to external ethyl groups are much broader and exhibits lower intensity for disordered film as compared to ordered ZnOEP film further highlighting the influence of molecular order on vibrational properties of the film. Moreover, Bader analysis of charge density reveals the formation of weak ionic-like inter-molecular interactions between protons belonging to the CH_3 moieties in different lattice planes. Such interactions are not anticipated for disordered film with randomly oriented ZnOEP molecules, justifying that intermolecular interactions are prevalent for ordered ZnOEP film which can have significant implications on the charge transport properties of ZnOEP films. Thus, differences in molecular packing lead to significant changes in intermolecular interactions, which are revealed by the Raman spectra. In order to establish structural deformations related to (C_β, C_m, C_α) for the as deposited ZnOEP TFs detailed structural analysis is needed to shed more light on this issue. We address this issue in next section devoted to comprehensive X-ray absorption analysis.

XAFS measurements at the Zn K edge were performed in both the near edge (X-ray Absorption Near edge Structure, XANES also named Near Edge X-ray Fine Structure NEXAFS in the literature) and extended energy range (Extended X-ray Absorption Fine Structure, EXAFS) on the different ZnOEP TF samples and a bulk polycrystalline ZnOEP one taken as a reference. Details on the data reduction and analysis are given in the supporting information SI-3. EXAFS spectra were measured at various orientations with respect to the linearly polarized x-ray beam, by varying the angle between the sample plane and the x-ray wave-vector (inset of Fig. 4), in order to probe linear dichroism effects. In Fig. 4 we report as the continuous lines the magnitudes of the Fourier Transforms, obtained in the range k= 2.8-7.5 $Å^{-1}$. A qualitative inspection indicates that the local structure of the films is rather similar to that of the bulk. However, the amplitude of the signals is significantly lower in the spectra of the annealed TF measured at θ=20° and θ=30° relative to the others. As discussed in the following the Zn K edge XANES spectra (Figure SI-4)

show a clear dependence from the experiment geometry, strongly suggesting that annealing induces an average orientational ordering of the molecular units composing the TF. This qualitatively explains the origin of the reduction of the amplitude of the EXAFS oscillations.

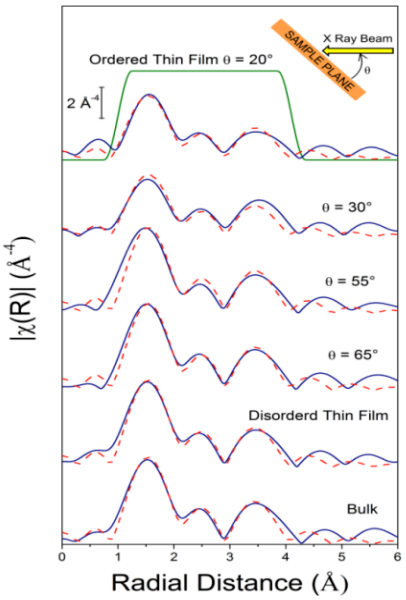

Fig. 4: Magnitude of the Fourier Transforms of EXAFS signals weighted by k^3. The continuous blue lines are the experimental data while the dashed red lines are the fits obtained as described in the text. The fitting window on the top is the same for all data.

Analysis of the EXAFS spectra in this peculiar system required an original approach, similar to that used in case of transition metal phtalocyanines[22]. The fits of the data are reported as dashed lines in Fig. 4 and listed in Table SI-4. The model structure is taken from ref. 20. The conclusion of the data analysis is that, within the uncertainties, the local structure (inter-atomic distances and Debye Waller (DW) factors of the bulk and films are very similar; DW factors for all samples and orientations generally increase with path length. In order to empirically take into account the variation of the EXAFS amplitudes for the ordered TF sample with orientation, we used a multiplicative factor β, which we found to decrease with decreasing θ. however, it does not follow the ideal $\sin^2\theta$ dependence, indicating a degree of disorder in the alignment of the macrocycle plane with respect to the substrate.

The fig 5(a) depicts the Zn K edge spectrum normalized at 9720 eV for the ordered, semiordered and disordered samples taken at the magic angle 55°.In case of disordered film the line shape of peak D appears distinct while peak L around 9660 eV shows notable decrease in intensity. N K edges (Fig.5b) were taken on the same ex-situ grown samples. No valuable differences were found in the XAS of in-situ grown samples. A slight shift in the Lowest Unoccupied Molecular Orbital (LUMO) position and a general broadening is detected for disordered films as compared to semiordered and ordered films for N K edge spectra. The feature D above the N K edge appears distinct for the disordered sample. The spectral line shape is in agreement with the data reported in the literature[39] with the feature labeled L corresponding to the transition to the (LUMO). Based on our multiple scattering (MS) calculations (SI-4.1 section, Fig. SI-3) we have assigned the sharp L peak as due purely to transitions to the π^* LUMO, while the second feature is a combination of the upper orbitals LUMO+1 and LUMO+2. The common procedure to extract the average molecular orientation in molecular layers employs the LUMO dichroism of light Z elements K edge XANES (also called NEXAFS in the literature or light atoms) data collected at several incident angles[40]. In Zn K edge and N K edges of the ordered and semiordered samples, the angular variations of the 1s to π^* transition LUMO intensity indicate an oriented resonance, evidenced by its systematic variation with incident angle Figure SI-4.

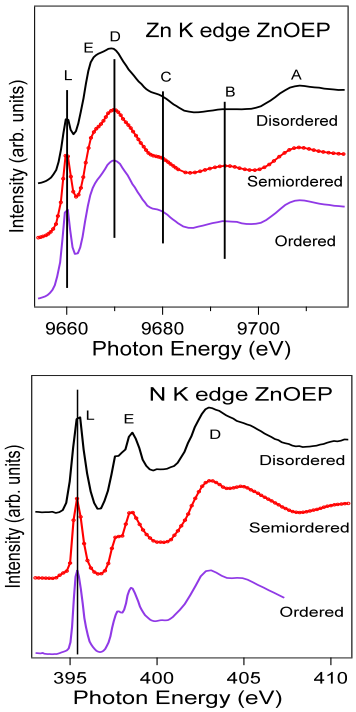

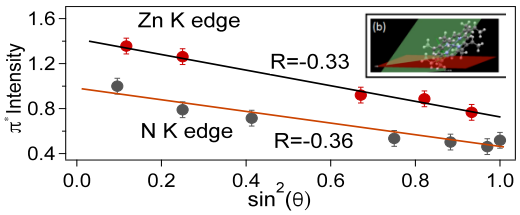

Fig. 5.(a) Normalized Zn K edges (b) N K edges XANES spectra of TF ZnOEP samples. Assignments of N K edge are indicated, following reference [8] (c) analysis of the LUMO intensity versus grazing angle in both the edges.

More details on the LUMO dichroism and the evaluation procedure are provided in the SI-4. We followed (SI-4.2) the well established procedure adopted for organic films, where the dichroic ratio R is used, to determine the average tilt molecular angle in TFs. Our quantitative analysis, taking into account the different light polarization in case of Hard X-rays Zn data (GILDA-LISA P ≈95%) and soft X-rays N spectra (BACH P=100%), found agreement from the two edges. For ordered ZnOEP TF, we observe a negative R factor of -0.33 to -0.36. If these films were completely crystalline, with a single crystal orientation, this tilt could be interpreted as a macrocycle plane tilt of ≈ 44° with respect to substrate. For semiordered samples analogous analysis provides an average angle of about 50° (Fig. SI-5). In the ZnOEP triclinic structure the macrocycle lies at about 45° with respect to the (1 0 0) plane and about 46° to the (01-1) plane, (Fig. 5 bottom). Hence in case of ordered film the triclinic cell present the [01-1] planes almost parallel to the substrate plane (as confirmed by GIXRD). This value of average tilt angle for semiordered sample is in good agreement with the results discussed in ref 7. N K edges for the three differently ordered films are almost similar,suggesting that macrocycle structural variations are feeble. The result is complementary to the Raman spectroscopy observation where no significant Raman shift has been observed for macrocycle vibrational modes.

EXAFS analysis found that the distances in the macrocycle within 3.5 Å from the central Zn result weakly perturbed within the error. In ordered films the factor β decreases with decreasing θ however, it does not follow the ideal $\sin^2\theta$ dependence, indicating a degree of disorder in the alignment of the macrocycle planes with respect to the substrate in the crystallites. The macrocycle in the disordered TF has a slightly expanded structure and higher DW factors compared to both the bulk and the ordered TF. FY and TEY N K edge spectra of *in-situ* and *ex-situ* ZnOEP TF did not show any difference, indicating identical and uniform composition of the samples No differences between *in-situ* and freshly grown *ex situ* samples exposed to air and subsequent measured in UHV were observed. Only a weak oxygen contaminant was detected within the photoemission sensitivity in the freshly grown *ex-situ* samples[41] limited to the first two layers of the films.

We applied the Full MS analysis to the XANES of the Zn central atom in order to enlighten the structural differences in the studied films. To get further indication on the structural effects of long-range order in the ZnOEP shells beyond the 4th, i.e. of the peripheral C atoms and ethyl groups, we finally performed structural MXAN fits of the Zn K edges, Results are shown in Fig. 6. Though XANES provides the averaged data within the films, the fits provide useful indications on the structural changes related to the differences in the XANES line shapes among the samples. We start with the fit of the bulk spectrum in order to define the potential calculated details. Then the magic angle spectra of the films have been fitted adopting the structural coordinates as fitting parameters. As first fit trial the EXAFS result has been adopted, multiplied by the β factor of Table SI-4, up to the atoms at distances of about 3.4 Å while the other coordinates has been taken according to ref. 20. Then two different coordinate models have been used: the single molecule (SM TR) of Fig. 1b, and the TR structural model consisting in the addition of the nearest C and N atoms (Fig.1 c) of the top and bottom ZnOEP molecules within the triclinic structure. Namely the coordinates of the C_β, C_1 and C_2 atoms together with the nearest neighbor molecule atoms N_{up}, N_{down}, $C_{\alpha\ up/down}$, $C_{m\ up/down}$, are taken as variables of the fit procedure, while the N C_α and C_m atoms are fixed from the EXAFS analysis. The starting trial from the EXAFS model are shown in fig. 6, the resulting likelihood parameter R_{sq} ranging between 0.98 e+2 and 0.32 e+2, as indicated in Fig. 6. The resulting fit quality is good for the disordered sample with R_{sq} sensibly decreased with respect to the EXAFS model. Both SM TR and TR model fits indicate that the C_1 and C_2 ethyl groups present a broaden distribution of distances in a sort of confusion ring (Table 4) confirming the Raman

observation related to peripheral ethyl groups vibrations. The different intermolecular paths result not strongly relevant and the SM TR structure is sufficient to get a good fit. In fact the best fit is obtained for TR model, though the agreement results similar to the SM TR. In case of TR model the addition of intermolecular/interplanar distances N_{up}/N_{down} and $C_{\alpha}{}_{up/down}$ results in a reduction of approximately 3%.

Even in the ordered TF data set the resulting fit quality improves with respect to the EXAFS model. The TR fits result improved with respect to the SM. The generally worst quality of the resulting SM TR fits for all the spectra taken at different grazing angles implies the extension of the structural input cluster to the TR structure, that models intermolecular interactions. Good quality simulations for the ordered ZnOEP TF are obtained for angle 55°, i.e. including in planes macrocycle, indicating that the outer C atoms (C_{α}, C_{β}) present a deformed symmetry. In particular for 20° and 30° spectra the EXAFS simulations found a very poor agreement. A single structural solution for the spectra at 20°, 30° and 55° has been obtained as best fit in both models. The average of C_{β} distances remain practically unchanged, though a weak reduction of the square symmetry (C_{4v}) of the C_{β}, shell is found, with longer distances along the X direction (see inlet in Table 2) in the plane of macrocycle.

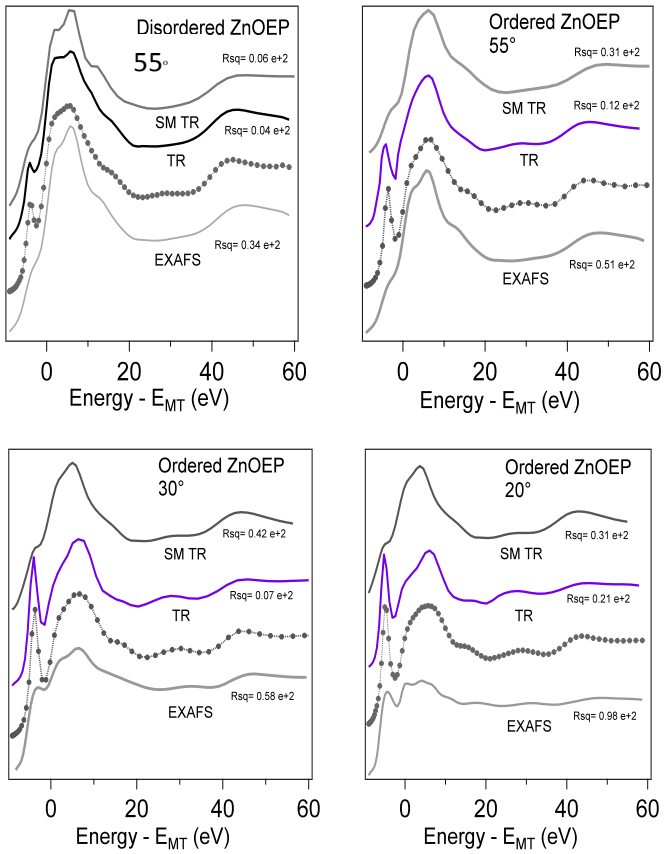

Figure 6: Comparison of the Zn K edge spectra (dots) and the MXAN simulations for the disordered and ordered films taken at magic angle at about 55°(top panel) and (bottom panel)at 20° and 30°. Solid lines curves are the simulations obtained from the structure extracted from EXAFS analysis (gray lines) and best fits obtained by the optimization of the outer C atoms shells in the triclinic structure (TR) and in the single molecule (SM) structures. The Residual square (Rsq) value for each simulation is also reported.

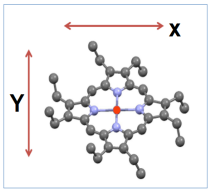

		Disordered	Disordered	Semi-Ordered	Ordered	Ordered
Model	EXAFS	SM TR	TR	SM TR	SM TR	TR
Best Fit Rsq Parameter	-	**0.06 e 2**	**0.04 e 2**	**0.4 e2**	**0.31 e 2**	**0.12 e2**
Zn-C, /Å	**4.3**	**4.29 along X** **4.31 along Y**	**4.29 along X** **4.30 along Y**	**4.26 along X** **4. 34 along Y**	**4.29 along X** **4.33 along Y**	**4.24 along X** **4. 36 along Y**
Nup-Ndown /Å	**3.59**	-	**3.48**	**3.51**	-	**3.55**
C_{α}up-C_{α}d /Å	**3.34**	-	**3.2**	**3.30**	-	**3.36**
Zn-C1 /Å	**5.63**	**Confusion** 5.93 along X 5.53 along Y	**Confusion** 5.87 along X 5.55 along Y	**5.93 along X** **5.37 along Y**	**5.95 along X** **5.32 along Y**	**5.84 along X** **5.50 along Y**
Zn-C2/ Å	**6.33 along X** **6.13 along Y**	**Confusion** 6.58 along X 6.20 along Y	**Confusion** 6.57 along X 6.12 along Y	**6.47 along X** **6.00 along Y**	**6.47 along X** **6.00 along Y**	**6.42 along X** **6.03 along Y**

Table 2 List of the ZnOEP distances in Å, as found by the structural MXAN fit by using the different models described in the text (see Fig.1). The X and Y directions are described in the inlet. Confusion indicates a substantial insensitivity of the simulation to the ethyl C_1 and C_2 coordinates.

The C_1 and C_2 ethyl groups present increased distances along the X direction with respect to the variations found along the Y direction, at variance to the distance distribution obtained in the

disordered case. The structural TR fit results sensibly improved with respect to the SM model confirming that the C_β, C_1 and C_2 atoms reduce their symmetry. Moreover the intermolecular distances of the nearest molecules ($N_{up/down}$ and $C_{up/down}$ atoms) result less perturbed than in the disordered case. The fits performed at angles closer to the normal i.e. for scattering paths including molecules belonging to different planes of the triclinic structure, present a worst fit quality and a no unambiguous solution of the structural simulations is obtained. Similar procedures and findings have been obtained for the semiordered spectra and reported in table 2.

Discussion

It is evident from Fig.7(a) that ordered stacking of molecules favours substantial π-π interactions. The calculated charge density contours depict the influence of π electron cloud on the neighbouring molecules in the triclinic ZnOEP framework as shown in fig 7(b). Small Raman shifts observed in the higher frequency range corresponding to skeletal carbon atoms (C_β, C_m, C_α) for the ordered films as compared to disordered film can be attributed to alterations of π charge density. It has been reported that molecular stacking induced alterations in the π charge density can lead to minor Raman shifts for the prophyrin thin films[36].

The structural MXAN fits of the Zn K edges reveal that spectral features for the disordered film can be reproduced considering 25 atoms instead of 31 atoms for ordered film in the calculation as indicated by the shell by shell analyses in Fig.SI-3. It suggests that structural orientation of ethyl groups (C_1, C_2) with respect to C_β becomes less significant for the disordered film. The Raman analysis appears to complement this observation as the two peaks at 225cm^{-1} and 245cm^{-1} corresponding to $C_\beta C_1 C_2$ vibrations are distinguishable for ordered film spectrum while these peaks disappear for disordered film spectrum as shown in fig.3a revealing that impact of random orientations corresponding to ethyl groups (C_1,C_2) for disordered film. The observation highlights the influence of molecular order on electronic and vibrational properties of the molecular films.

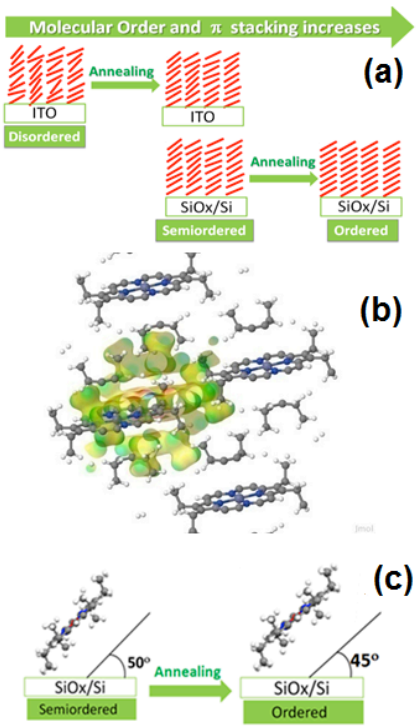

Figure 7 (a) Schematic representation of enhanced molecular order of ZnOEP molecules depending on substrate and annealing (b) Charge contours as calculated in the triclinic ZnOEP structure between neighbour molecules (c) Schematic representation of ZnOEP molecular orientation for semiordered and ordered films based on XANES analysis.

In addition, our detailed MXAN fitting analysis of near edge XAFS establishes a symmetry reduction in the molecular conformer involving C_β and C_α carbon atoms highlighting the consequences of increased π stacking of ZnOEP molecules adopting triclinic structure. Such a strain in the structure is not observed for macrocycle as shown in Table 2. These observations compliment Raman analysis where no Raman shift has been observed for the vibrational modes involving macrocycle while small but detectable Raman shift has been observed for the skeletal carbon atoms vibrational modes for the ordered film as compared to semiordered and disordered film.

Comparison of GIXRD reflections integrated in the 80°-100° range angle shows a slight progressive increasing in cell parameter as shown in Fig 8. There is a trend of small but notable shift of the features related to 001, 010 and 01-1 as molecular order improves from disordered to ordered film. These results indicate that the film crystallites have a preferential growth orientation close to the

perpendicular (01–1) plane direction. Nonetheless, GIXRD is here employed to enlighten the structural and morphological differences in the samples evaluated by XAFS. The match of GIXRD patterns with simulations aimed at the evaluation of the prevalent orientation of crystallites. Assuming the (01-1) as the preferential growth direction this orientation corresponds to 01-1 lattice plane of the single crystal parallel to the Silicon substrate plane.

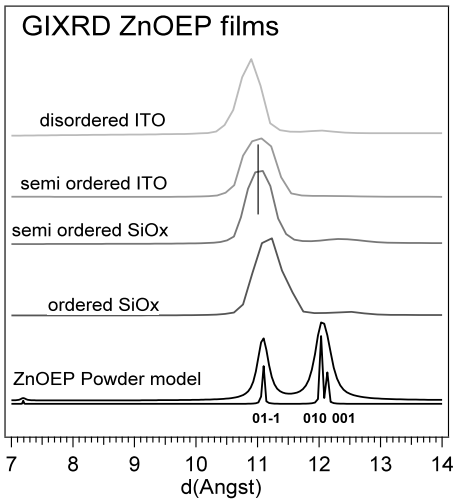

Fig.8 GIXRD reflections integrated in the 80°-100° range. The indexing has been assigned through the powder simulated XRD pattern (Mercury code) from published data 25

It has been reported based on XRD analysis that ZnOEP TF of 40nm thickness on SiOx/Si exhibits one type of crystallites having diffraction plane parallel to substrate with ZnOEP molecules in crystallites inclined by 50° with respect to substrate.[7] These observations are in good agreement with ours, although the interplanar separation results (Fig.8) slightly reduced for semiordered and disordered film (see also Table 1). These results are in coherence with observation that the XRD results of semiordered ZnOEP films on SiOx/Si substrate have good resemblance with those on ITO/glass. At variance with the semiordered film, we obtained an angle of about 45° for the ordered film with respect to substrate. It appears that annealing of ZnOEP thin film deposited on SiOx/Si at 80°C improves the order along with small but notable change in angle of orientation as shown in fig.7(c).

EXAFS fitting analysis establishes that there is stretching of skeletal carbon atoms for the ordered film which may lead to unsymmetrical stretching of π conjugated system of porphyrin ring, thereby impacting HOMO-LUMO gap and optical absorption properties. The probable cause of such unsymmetrical stretching of skeletal carbon can be intermolecular interactions due to proximity with neighboring molecules in the triclinic framework. Such alterations of the π conjugation netwrok are not expected for disordered film grown on ITO at room temperature. Thus, we anticipate higher cell efficiency for the ordered ZnOEP thin films on SiOx/Si obtained by annealing films grown at room temperature.

Conclusions

Summarizing, our work highlights the consequences of different degree of long range order by considering ZnOEP thin films grown on SiOx/Si and ITO substrates with different roughness by UHV vapor deposition with or without subsequent annealing. GIXRD analysis reveals that ZnOEP films present different degree of long-range ordering, paracrystallinity and average crystallites size. Although remarkable differences are found in the intramolecular reorganization, the effect of the disorder being mainly related to the skeletal carbon atom C_α, C_β and C_1, C_2 outer shell displacements. The macrocycle and the C atoms up to distances < 4 Å remain almost unperturbed for ordered and disordered films, though slight differences within the error are found by EXAFS. The Nitrogen surrounding remains practically unperturbed, as also shown by N K edge NEXAFS. The study provides useful insights for the creation and control of functional molecular films, crucial for the technological applications of organic semiconductors.

Acknowledgements

S.C. and M.P. acknowledge the COST EuSpec. D.N. acknowledges CBM scrl for providing access to the BioNanoAnalysis core facility. This work is based on measurements taken after BACH ELETTRA 20130071 and 20140293 and GILDA ESRF 08-01 9452013 proposals. Project partially supported by the Italian MIUR through the Progetto PIK EXPROREL and Eurofel. The CNR-IOM technical staff, Federico Salvador, Paolo Bertoch, Davide Benedetti and Andrea Martin, is kindly acknowledged for their support.

Conflicts of interest

There are no conflicts to declare.

References

[1] Y.-Y. Noh, J.-J. Kim, Y. Yoshida, K. Yase, *Adv. Matter.* 2003, 15, 699-702.

[2] Imahori et al. , *Accounts of Chemical Research*, 2009, 42, 1809-1818.

[3] Anh D. Phan, Phys. Review E 2014, **90**, 062707.

[4] Perng, J.-H., Bocian, D.F. Journal of Physical Chemistry, 1992, 96 (12), 4804-4811.

[5] L. Edwards, D. H. Dolphin, M. Gouterman, *J. of Molecular Spectrocopy* 1970, 36, 90-109.

[6] S. Ryuzaki and J. Onoe , *J. Appl. Phys.,*2008*,* **103**, 033516.

[7] S. Ryuzaki, T. Hasegawa, J. Onoe, *J. Appl. Phys.,* 2009, 105, 113529.

[8] S. Ryuzaki, T. Kai, Y. Toda, S. Adachi, J. Onoe, *J. Phys. D: Appl. Phys.*, 2011, 44, 145103.

[9] R. Noriega, J. Rivnay, K. Vandewal, F. P. V. Koch, N. Stingelin, P. Smith, M. F. Toney, A. Salleo, *Nature Materials,* 2013 12, 1038-1044.

[10] Y. Gao, *Materials Science and Engineering* , 2010, R68, 39–87

[11] J. L. Brédas, J. P. Calbert, D. A. da Silva Filho, J. Cornil, *Proc. Natl. Acad. Sci. U.S.A.,* 2002, 99, 5804-5809.

[12] T. Minari, M. Seto, T. Nemoto, S. Isoda K. Tsukagoshi, Y. Aoyagi, *Applied Physics Letters* , 2007, 91, 123501.

[13] M. Campione, E. Fumagalli, L. Raimondo, A. Monguzzi, F. Meinardi, A. Sassella Chem. Mater. 2011, 23, 832–840.

[14] Jia-Mei Yang, Feng-Xia Wang, Ge-Bo Pan, Nanoscale, 2016, 8, 2811.

[15] Heng-Xing Ji,ab Jin-Song Hua and Li-Jun Wan, *Chem. Commun.,* 2008, 0, 2653–2655.

[16] Yan Xiao, Feng-Xia Wang, Jia-Mei Yang, Miao-Rong Zhang, Ge-Bo Pan, *Scientific Reports*, 2017, 7, 9838, 2917.

[17] Feng-Xia Wang, Yong-Qiang Liu, Hao-Di Wu, Yan Xiao, Ge-Bo Pan, *J. Mater. Chem. C*, 2013, 1, 422–425.

[18] J. Onoe, S. Watanabe, S. Kato, M. Nakaya, J.-P. Bucher *J.Chem.Phys.,* 2017, 147,214701.

[19] Callot, H. J.; Ocampo, R. The Porphyrin Handbook; Academic Press: New York, 2000; Vol. 1.

[20] A. Ozarowski, L. Hon Man, and A. L. Balch, *J. Am. Chem. Soc.*, 2003, 125, 12606-12614.

[21] M. Okazaki, C.A. McDowell, *J. Am. Chem. Soc.* 1984, 106,3185−3190; L. Frydman, A.C. Olivieri, L.E. Diaz, A.Valasinas, B. Frydman, *J. Am. Chem. Soc.* 1988, 110, 5651−5661; Ji HX, Hu JS, Wan LJ., *Chem Communications*, 2013; 23, 2653–2655.

[22] G. Rossi, F. d'Acapito, L. Amidani, F. Boscherini, M. Pedio *Phys. Chem. Chem. Phys.,* 2016, 18, 23686-23694.

[23] F. d'Acapito et al., *ESRF Newsletter* , 1998, 30, 42; S. Pascarelli, F. Boscherini, F. d'Acapito, J. Hrdy, C. Meneghini, and S. Mobilio, *J. Synchrotron Radiat.*, 3, 147 (1996).

[24] G. Ciatto, F. d'Acapito, F. Boscherini, and S.Mobilio, *J. Synchrotron Radiation*, 2004, 11, 278 .

[25] M. Zangrando, M. Zacchigna, M. Finazzi, D. Cocco, R. Rochow and F. Parmigiani, *Rev. Sci. Instrum.*, 2004, 75, 31–36.

[26]G. Drera, G. Salvinelli, J. Åhlund, P. G. Karlsson, B. Wannberg, E. Magnano, S. Nappini and L. Sangaletti, *J. El. Spect. Relat. Phen.*, 2014, 195, 109–116.

[27] M.Benfatto, S. Della Longa, *J. Synch. Rad.*, 2001 8, 1087-1094.

[28] M. Benfatto, S. Della Longa, *J.Phys. Conf. Ser.*, 2009, 190, 12031

[29] A. Lausi, M. Polentarutti, S. Onesti, J. R. Plaisier, E. Busetto, G. Bais, L. Barba, A. Cassetta, G. Campi, D. Lamba, et al., *Eur. Phys. J. Plus* , 2015, 130, 1–8.

[30] G. Scavia, L. Barba, G. Arrighetti, S. Milita, W. Porzio *European Polymer Journal* , 2012, 48, 1050–1061.

[31] A. M. Hindeleh, R. Hosemann, *J Mater Sci* 1991, 26, 5127–5133; R Hosemann, A.M Hindeleh*, J. Macromol. Sci. Phys. B*, 1995, 34, 327–336.

[32] J.R. Ares, A. Pascual, I.J. Ferrer, C. Sánchez, *Thin Solid Films* , 2005, 480, 477.

[33] A. Kumar, D. Naumenko, L. Cozzarini, L. Barba, A. Cassetta, M. Pedio, *J. Raman Spectroscopy*, 2018, SPECIAL ISSUE, 1-8.

[34] Perng, J.-H., Bocian, D.F. Journal of Physical Chemistry, 1992, 96 (12), 4804-4811.

[35] M. Abe, T. Kitagawa, Y. Kyogoku, *The Journal of Chemical Physics*, 1978, 69, 4526.

[36] L. D. Sparks, W. R. Scheidt, and J. A. Shelnutt, *J. Am. Chem. Soc.*, 1988, 110, 12.

[37]D. Melamed, B. Darlington, D. J. R.Brook,H.L. Pan, A. Campion, M. A. Fox, *J. Phys. Chem.*, 1994, 98, 8971-8976

[38] N. Coppede, T. Toccoli, A. Pallaoro, F. Siviero, K. Walzer, M. Castriota, E. Cazzanelli, S. Iannotta, *J. Phys. Chem. A* , 2007, 111, 12550-12558.

[39] C. S. Guo, L. Sun, K. Hermann, C. F. Hermanns, M. Bernien, W. Kuch, *J. Chem. Phys.* , 2012, 137, 194703.

[40] D. M. DeLongchamp , R. J. Kline , D. A. Fischer , L. J. Richter, M. F. Toney, *Adv. Mater.*, 2011, 23, 319–337.

[41]Aged samples contrary to the short term air exposure samples show C1s broadening and Oxygen contamination with the O1s data due to coexistence of molecular oxygen and water vapour from the atmosphere.